Supporting Information for: Porosity-Permeability Relationships in Mudstone from Pore-Scale Fluid Flow Simulations using the Lattice Boltzmann Method

Harsh Biren Vora[1], Brandon Dugan[2]

[1]Department of Earth, Environment and Planetary Sciences, Rice University, Houston, TX 77005

[2]Department of Geophysics, Colorado School of Mines, Golden, CO 80401

Contents of this File:

Text S1

Figures S1 and S2

Tables S1 to S4

Introduction:

This supporting information includes six parts:

(1) Compaction data from smectite, kaolinite and intermediate mudstone models [Table S1]

(2) Evolution of vertical tortuosity (τ_v) during compaction and fluid injection [Fig S1]

(3) Incorporating heterogenous platelet geometry in mudstone models [Text S1 and Fig. S2]

(4) Compaction data from NM1 and NM2 models [Table S2]

(5) Microfracture growth data in compacted intermediate mudstone model [Table S3]

(6) Macrofracture propagation data in compacted intermediate mudstone model [Table S4]

Table S1: Vertical (q_v) and horizontal (q_h) flux during compaction of kaolinite, smectite and intermediate mudstone models, simulated by step-wise decrease in intrabed (ξ) and interbed pore throat diameters (λ).

Model	Step	*Porosity* ϕ	Intrabed Pore Throat Width ξ	Interbed Pore Throat Width λ	Platelet Orientation Θ	Vertical Flux q_v	Reynolds Number Vertical flow Re_v	Vertical Permeability k_v	Vertical Tortuosity τ_v	Horizontal Flux q_h	Reynolds Number Horizontal flow Re_h	Horizontal Permeability k_h	Horizontal Tortuosity τ_h
			(nm)	(nm)	Degrees	(m/s)		(m^2)		(m/s)		(m^2)	
Kaolinite	1	0.76	3.60×10^{2}	3.60×10^{2}	45	7.15×10^{-1}	2.41×10^{0}	8.31×10^{-15}	1.02	1.12×10^{-1}	1.88×10^{-2}	1.10×10^{-14}	6.56
Kaolinite	2	0.68	2.60×10^{2}	2.60×10^{2}	35	3.56×10^{-1}	1.20×10^{0}	3.42×10^{-15}	1.02	5.16×10^{-2}	8.69×10^{-3}	4.96×10^{-15}	7.05
Kaolinite	3	0.58	1.80×10^{2}	1.80×10^{2}	25	9.81×10^{-2}	3.31×10^{-1}	7.84×10^{-16}	1.03	1.77×10^{-2}	2.99×10^{-3}	1.68×10^{-15}	5.71
Kaolinite	4	0.46	1.20×10^{2}	1.20×10^{2}	20	2.63×10^{-2}	8.85×10^{-2}	1.78×10^{-16}	1.12	9.27×10^{-3}	1.56×10^{-3}	8.67×10^{-16}	3.17
Kaolinite	5	0.35	8.00×10^{1}	8.00×10^{1}	15	5.73×10^{-3}	1.93×10^{-2}	3.42×10^{-17}	1.15	2.33×10^{-3}	3.93×10^{-4}	2.16×10^{-16}	2.83
Kaolinite	6	0.28	6.00×10^{1}	6.00×10^{1}	10	1.92×10^{-3}	6.49×10^{-3}	1.07×10^{-17}	1.19	8.69×10^{-4}	1.47×10^{-4}	8.02×10^{-17}	2.63
Kaolinite	7	0.19	4.00×10^{1}	4.00×10^{1}	5	3.91×10^{-4}	1.32×10^{-3}	2.02×10^{-18}	1.37	2.60×10^{-4}	4.39×10^{-5}	2.39×10^{-17}	2.06
Kaolinite	8	0.14	4.00×10^{1}	4.00×10^{1}	0	1.23×10^{-4}	4.14×10^{-4}	6.33×10^{-19}	2.06	1.56×10^{-4}	2.63×10^{-5}	1.43×10^{-17}	1.62
Smectite	1	0.80	9.00×10^{0}	9.00×10^{0}	45	3.56×10^{-1}	4.00×10^{-2}	6.84×10^{-17}	1.01	4.18×10^{-2}	9.40×10^{-5}	1.33×10^{-16}	8.64
Smectite	2	0.76	7.00×10^{0}	7.00×10^{0}	35	2.10×10^{-1}	2.36×10^{-2}	3.61×10^{-17}	1.06	5.08×10^{-2}	1.14×10^{-4}	1.60×10^{-16}	4.37
Smectite	3	0.72	5.00×10^{0}	5.00×10^{0}	25	1.08×10^{-1}	1.21×10^{-2}	1.63×10^{-17}	1.14	4.11×10^{-2}	9.24×10^{-5}	1.29×10^{-16}	2.98
Smectite	4	0.66	4.00×10^{0}	4.00×10^{0}	15	3.50×10^{-2}	3.93×10^{-3}	4.60×10^{-18}	1.20	1.66×10^{-2}	3.72×10^{-5}	5.16×10^{-17}	2.54
Smectite	5	0.58	3.00×10^{0}	3.00×10^{0}	10	5.02×10^{-3}	5.64×10^{-4}	5.59×10^{-19}	1.34	3.18×10^{-3}	7.15×10^{-6}	9.85×10^{-18}	2.12
Smectite	6	0.45	2.00×10^{0}	2.00×10^{0}	5	3.04×10^{-4}	3.42×10^{-5}	2.77×10^{-20}	1.64	2.79×10^{-4}	6.28×10^{-7}	8.59×10^{-19}	1.78
Smectite	7	0.16	1.00×10^{0}	1.00×10^{0}	0	1.84×10^{-7}	2.06×10^{-8}	1.30×10^{-23}	2.56	3.06×10^{-7}	6.88×10^{-10}	9.35×10^{-22}	1.54
General	1	0.73	13.71×10^{1}	13.71×10^{1}	45	1.39×10^{-1}	3.12×10^{-1}	6.10×10^{-16}	1.02	1.75×10^{-2}	1.12×10^{-3}	1.11×10^{-15}	8.06
General	2	0.66	10.28×10^{1}	10.28×10^{1}	35	3.73×10^{-2}	8.37×10^{-2}	1.38×10^{-16}	1.04	7.07×10^{-3}	4.54×10^{-4}	4.44×10^{-16}	5.46
General	3	0.60	80.00×10^{0}	80.00×10^{0}	25	1.73×10^{-2}	3.88×10^{-2}	5.59×10^{-17}	1.11	5.78×10^{-3}	3.71×10^{-4}	3.60×10^{-16}	3.31
General	4	0.50	57.14×10^{0}	57.14×10^{0}	20	6.95×10^{-3}	1.56×10^{-2}	1.93×10^{-17}	1.17	3.00×10^{-3}	1.93×10^{-4}	1.86×10^{-16}	2.71
General	5	0.44	45.71×10^{0}	45.71×10^{0}	15	2.98×10^{-3}	6.70×10^{-3}	7.58×10^{-18}	1.21	1.45×10^{-3}	9.31×10^{-5}	8.93×10^{-17}	2.50
General	6	0.35	34.28×10^{0}	34.28×10^{0}	10	1.06×10^{-3}	2.38×10^{-3}	2.45×10^{-8}	1.39	7.22×10^{-4}	4.64×10^{-5}	4.43×10^{-17}	2.04
General	7	0.25	22.85×10^{0}	22.85×10^{0}	5	2.48×10^{-4}	5.57×10^{-4}	5.16×10^{-19}	1.66	2.33×10^{-4}	1.49×10^{-5}	1.42×10^{-17}	1.77
General	8	0.07	11.42×10^{0}	11.42×10^{0}	0	5.54×10^{-6}	1.24×10^{-5}	1.02×10^{-20}	2.20	7.68×10^{-6}	4.93×10^{-7}	4.68×10^{-19}	1.59

Fig. S1: Vertical tortuosity (τ_v) (a) increases as porosity declines during compaction of kaolinite, smectite and intermediate mudstone models (b) declines with growth of microfracture network and macrofracture propagation during simulated fluid injection in compacted intermediate mudstone model.

a.

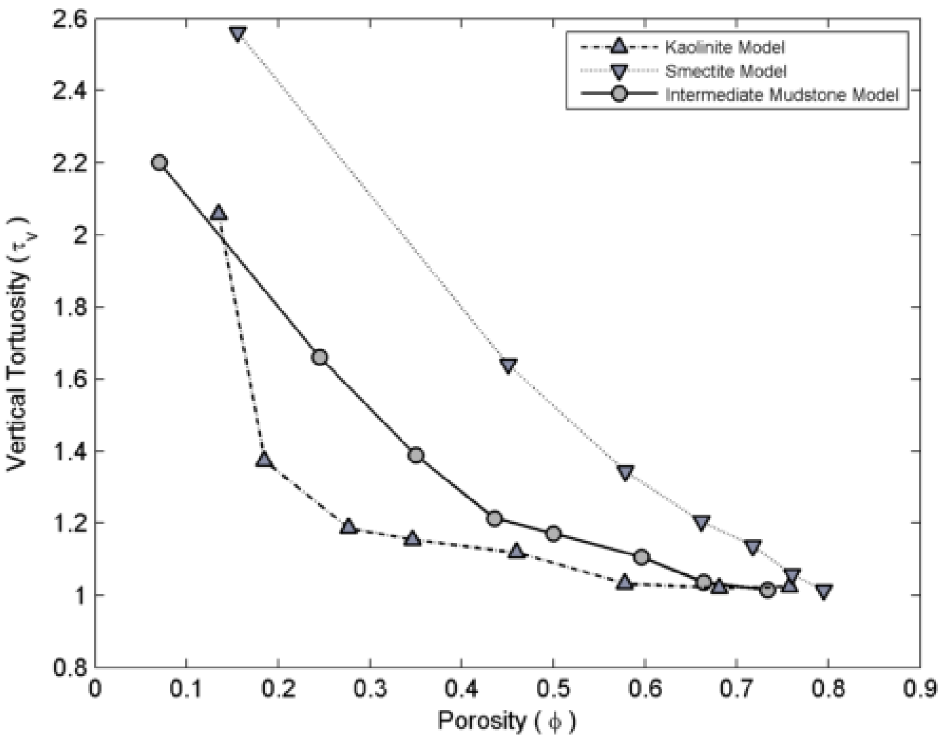

b.

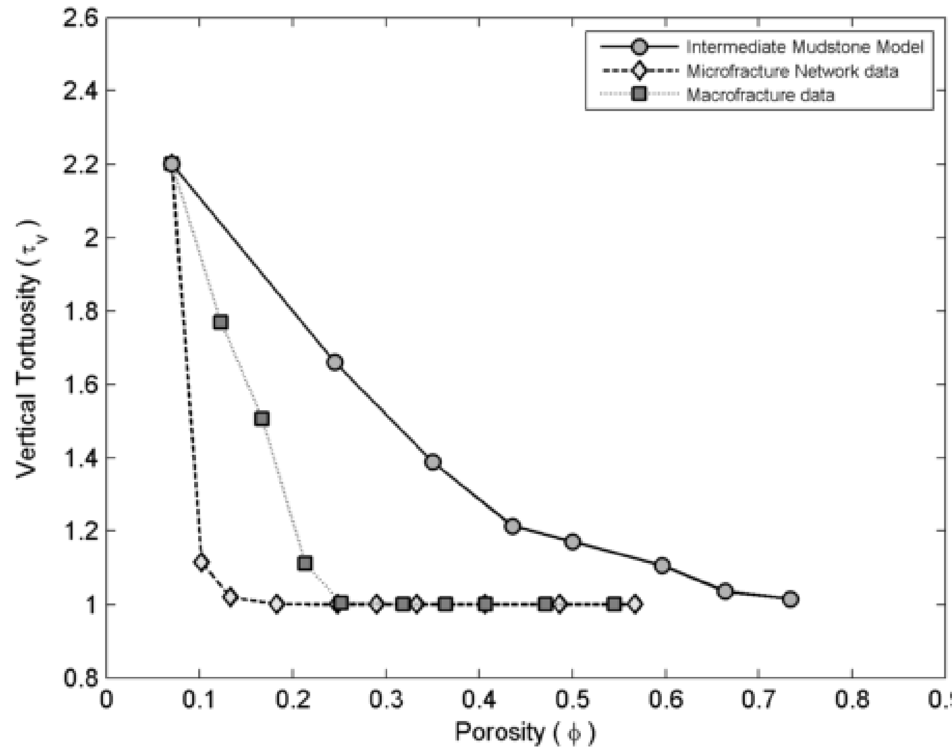

Text S1: **Incorporating heterogenous platelet geometry in mudstone models:** We employ inputs of mineral weight fractions of smectite, illite and chlorite to model the mudstone pore structures. We assume constant density of clay minerals; the modeled weight of each clay platelet can be calculated as $m\beta$ x $m\beta$ x β. The maximum number of smectite ($no_{smectite}{}^{max}$), illite ($no_{illite}{}^{max}$)and chlorite ($no_{chlorite}{}^{max}$) platelets in the models are calculated as:

$$no_{smectite}{}^{max} = [0.1\ \mu m * 0.1\ \mu m * 0.002\ \mu m]\ * input\ smectite\ wt\%, \qquad \text{(S1)}$$

$$no_{illite}{}^{max} = \ [2\ \mu m * 2\ \mu m * 0.1\ \mu m]\ * input\ illite\ wt\%, \qquad \text{(S2)}$$

$$no_{chlorite}{}^{max} = [2.5\ \mu m * 2.5\ \mu m * 0.1\ \mu m] * input\ chlorite\ wt\%. \qquad \text{(S3)}$$

The number of smectite ($no_{smectite}$), illite (no_{illite}) and chlorite ($no_{chlorite}$) platelets in a model are determined using the highest common factor (HCF) between $no_{smectite}{}^{max}$, $no_{illite}{}^{max}$ and $no_{chlorite}{}^{max}$ as:

$$no_{smectite} = {no_{smectite}^{max}}/_{HCF}, \qquad \text{(S4)}$$

$$no_{illite} = {no_{illite}^{max}}/_{HCF}\ , \qquad \text{(S5)}$$

$$no_{chlorite} = {no_{chlorite}^{max}}/_{HCF}. \qquad \text{(S6)}$$

The number of bedding layers is determined as the highest common factor (HCF_beds) between $no_{smectite}$, no_{illite} and $no_{chlorite}$. The minimum value of HCF_beds is three. The number of smectite, illite and chlorite platelets in each bedding layer is calculated as ($no_{smectite}/HCF\_beds$), (no_{illite}/HCF_beds) and ($no_{chlorite}/HCF\_beds$) respectively. Each bed is simulated by random three-dimensional spatial distribution of ($no_{smectite}/HCF\_beds$) smectite platelets, (no_{illite}/HCF_beds) illite platelets and ($no_{chlorite}/HCF\_beds$) chlorite platelets with intrabed pore throats of diameter ε between platelets. The simulated beds are stacked vertically with interbed pore throat of diameter λ to develop the unrotated mudstone model [Fig. S3]. The developed matrix is transformed by input grain orientation angle, Θ, to simulate the final mudstone model.

Figure S2: Scaled-down model of mudstone pore structure *NM2*, replicating mineralogy of natural sample 1324B-7H-7, at ϕ=0.79. The mudstone model consists of 31% smectite, 41% illite and 28% chlorite by volume (θ=0°). (a) Cross sectional view of *NM2* pore structure with smectite, illite and chlorite platelets; and (b) Orthogonal view of *NM2* with directions of vertical (q_v) and horizontal flow (q_h).

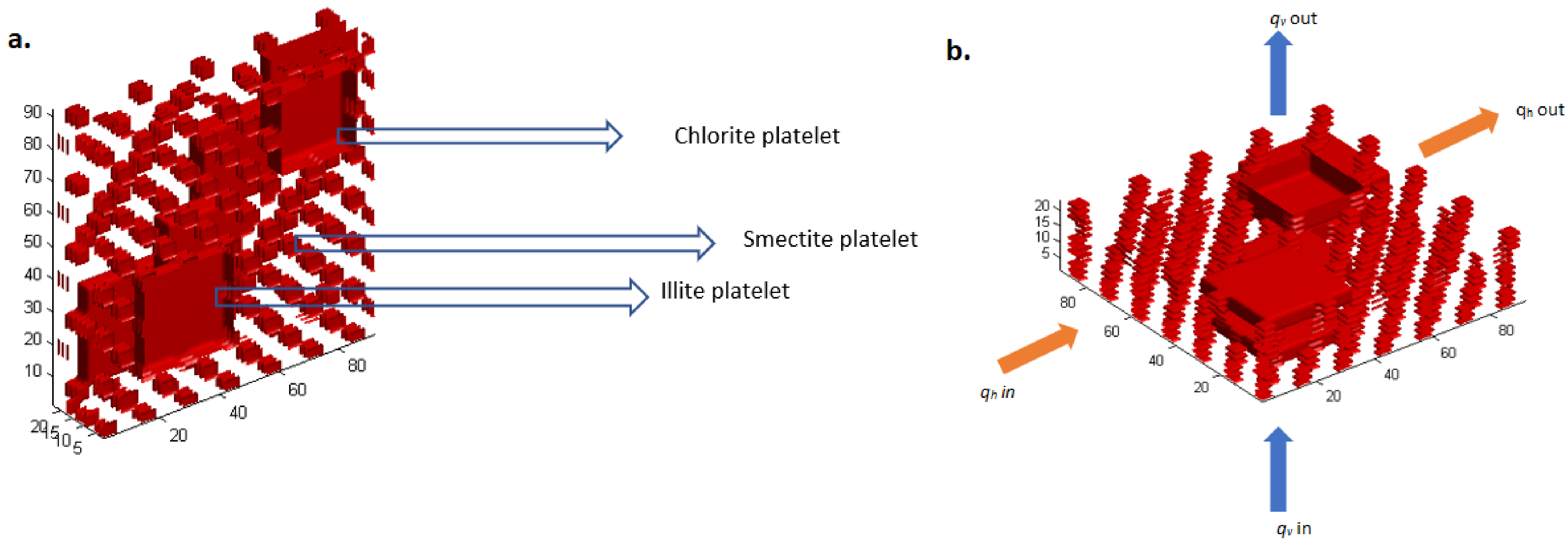
a.
Chlorite platelet
Smectite platelet
Illite platelet
b.
q_v out
q_h out
q_h in
q_v in

Table S2: Vertical (q_v) and horizontal (q_h) flux during compaction of *NM1* and *NM2* mudstone models, simulated by step-wise decrease in intrabed (ξ) and interbed pore throat diameters (λ).

Model	Step	*Porosity* ϕ	Intrabed Pore Throat Width ξ	Interbed Pore Throat Width λ	Platelet Orientation Θ	Vertical Flux q_v	Reynolds Number Vertical flow Re_v	Vertical Permeability k_v	Vertical Tortuosity τ_v	Horizontal Flux q_h	Reynolds Number Horizontal flow Re_h	Horizontal Permeability k_h	Horizontal Tortuosity τ_h
			(nm)	(nm)	Degrees	(m/s)		(m^2)		(m/s)		(m^2)	
NM1	1	0.72	5.05×10^{1}	5.05×10^{1}	15	5.03×10^{-2}	2.71×10^{-2}	1.54×10^{-16}	1.74	5.08×10^{-2}	7.42×10^{-4}	1.39×10^{-15}	1.73
NM1	2	0.67	3.85×10^{1}	3.85×10^{1}	10	1.90×10^{-2}	1.03×10^{-2}	5.19×10^{-17}	2.06	2.43×10^{-2}	3.55×10^{-4}	6.53×10^{-16}	1.62
NM1	3	0.60	2.65×10^{1}	2.65×10^{1}	6	3.94×10^{-3}	2.12×10^{-3}	9.39×10^{-18}	2.44	6.22×10^{-3}	9.08×10^{-5}	1.64×10^{-16}	1.55
NM1	4	0.49	1.45×10^{1}	1.45×10^{1}	3	3.36×10^{-4}	1.81×10^{-4}	6.86×10^{-19}	2.99	6.70×10^{-4}	9.78×10^{-6}	1.73×10^{-17}	1.50
NM1	5	0.32	2.5×10^{0}	2.5×10^{0}	0	4.17×10^{-6}	2.25×10^{-6}	7.09×10^{-21}	3.69	1.05×10^{-5}	1.53×10^{-7}	2.66×10^{-19}	1.47
NM2	1	0.58	6.25×10^{1}	6.25×10^{1}	12	1.41×10^{-2}	7.62×10^{-3}	3.11×10^{-17}	1.29	8.16×10^{-3}	1.19×10^{-4}	2.27×10^{-16}	2.23
NM2	2	0.50	3.85×10^{1}	3.85×10^{1}	9	3.13×10^{-3}	1.69×10^{-3}	6.65×10^{-18}	1.55	2.63×10^{-3}	3.85×10^{-5}	7.07×10^{-17}	1.85
NM2	3	0.45	2.65×10^{1}	2.65×10^{1}	6	1.31×10^{-3}	7.09×10^{-4}	2.74×10^{-18}	1.90	1.50×10^{-3}	2.19×10^{-5}	3.96×10^{-17}	1.66
NM2	4	0.37	1.45×10^{1}	1.45×10^{1}	3	3.16×10^{-4}	1.71×10^{-4}	6.46×10^{-19}	2.48	5.06×10^{-4}	7.39×10^{-6}	1.30×10^{-17}	1.55
NM2	5	0.25	2.5×10^{0}	2.5×10^{0}	0	2.39×10^{-5}	1.29×10^{-5}	4.79×10^{-20}	3.66	5.96×10^{-5}	8.71×10^{-7}	1.51×10^{-18}	1.47

Table S3: Vertical flux (q_v^{mf}) during growth of microfractures through compacted intermediate mudstone, simulated by step-wise increase in microfracture width (ξ^{mf}).

Step	***Porosity*** ϕ	**Micro-fracture Width** ξ^{mf}	**Effective Fracture Width** ε_{eff}^{mf}	**Interbed Pore Throat Width** λ	**Vertical Flux** q_v^{mf}	**Reynolds Number Vertical flow** Re_v	**Vertical Permeability** k_v^{mf}	**Vertical Tortuosity** τ_v^{mf}
		(nm)	(nm)	(nm)	(m/s)		(m^2)	
1	0.07	11.42 x10^0	0.00 x10^0	11.42 x10^0	5.54 x 10^{-6}	1.24 x 10^{-5}	1.02 x 10^{-20}	2.20
2	0.10	57.14 x10^0	1.37 x 10^2	11.42 x10^0	1.56 x 10^{-4}	3.52 x 10^{-4}	2.89 x 10^{-19}	1.11
3	0.13	10.20 x10^1	2.74 x 10^2	11.42 x10^0	1.05 x 10^{-3}	2.37 x 10^{-3}	1.95 x 10^{-18}	1.02
4	0.18	18.28 x10^1	5.14 x 10^2	11.42 x10^0	7.99 x 10^{-3}	1.79 x 10^{-2}	1.48 x 10^{-17}	1.00
5	0.25	29.71 x10^1	8.57 x 10^2	11.42 x10^0	4.68 x 10^{-2}	1.05 x 10^{-1}	8.66 x 10^{-17}	1.00
6	0.29	37.70 x10^1	1.10 x 10^3	11.42 x10^0	1.12 x 10^{-4}	2.52 x 10^{-1}	2.07 x 10^{-16}	1.00
7	0.33	46.85 x10^1	1.37 x 10^3	11.42 x10^0	2.47 x 10^{-1}	5.56 x 10^{-1}	4.57 x 10^{-16}	1.00
8	0.41	64.00 x10^1	1.89 x 10^3	11.42 x10^0	7.59 x 10^{-1}	1.71 x 10^0	1.40 x 10^{-15}	1.00
9	0.49	86.85 x10^1	2.57 x 10^3	11.42 x10^0	2.17 x10^0	4.88 x 10^0	4.01 x 10^{-15}	1.00
10	0.57	11.54 x10^2	3.43 x 10^3	11.42 x10^0	5.19 x10^0	1.17 x 10^1	9.59 x 10^{-15}	1.00

Table S4: Vertical flux (q_v^{frac}) during propagation of macrofracture through compacted intermediate mudstone, simulated by step-wise increase in fracture width (ξ^{frac}).

Step	***Porosity*** ϕ	**Macro-fracture Width** ξ^{frac}	**Effective Fracture Width** ε_{eff}^{frac}	**Interbed Pore Throat Width** λ	**Vertical Flux** q_v^{frac}	**Reynolds Number Vertical flow** Re_v	**Vertical Permeability** k_v^{frac}	**Vertical Tortuosity** τ_v^{frac}
		(nm)	(nm)	(nm)	(m/s)		(m^2)	
1	0.07	11.42 x10^0	0.00 x10^0	11.42 x10^0	5.54 x 10^{-6}	1.24 x 10^{-5}	1.02 x 10^{-20}	2.20
2	0.12	37.71 x 10^1	3.66 x 10^2	11.42 x10^0	9.41 x 10^{-6}	2.11 x 10^{-5}	1.74 x 10^{-20}	1.77
3	0.17	70.85 x 10^1	6.97 x 10^2	11.42 x10^0	1.17 x 10^{-5}	2.64 x 10^{-5}	2.17 x 10^{-20}	1.51
4	0.21	11.09 x 10^2	1.10 x 10^3	11.42 x10^0	3.83 x 10^{-4}	8.60 x 10^{-4}	7.07 x 10^{-19}	1.11
5	0.25	14.74 x 10^2	1.46 x 10^3	11.42 x10^0	5.81 x 10^{-3}	1.31 x 10^{-2}	1.07 x 10^{-17}	1.01
6	0.32	22.06 x 10^2	2.19 x 10^3	11.42 x10^0	6.64 x 10^{-2}	1.49 x 10^{-1}	1.22 x 10^{-16}	1.00
7	0.36	27.88 x 10^2	2.78 x 10^3	11.42 x10^0	3.00x10^0	6.75 x 10^0	5.55 x 10^{-15}	1.00
8	0.41	34.40 x 10^2	3.43 x 10^3	11.42 x10^0	7.36 x10^0	1.65 x 10^1	1.36 x 10^{-14}	1.00
9	0.47	45.83 x 10^2	4.57 x 10^3	11.42 x10^0	1.36 x 10^1	3.06 x 10^1	2.52 x 10^{-14}	1.00
10	0.55	62.97 x 10^2	6.29 x 10^3	11.42 x10^0	2.09 x 10^1	4.69 x 10^1	3.85 x 10^{-14}	1.00